Approximate analytical solutions to the double-stance dynamics of the lossy Spring-Loaded Inverted Pendulum

Mohammad Shahbazi[1,2,*], Uluç Saranlı[3], Robert Babuška[1], Gabriel A. D. Lopes[1]

Abstract

This paper introduces approximate time domain solutions to the otherwise non-integrable double-stance dynamics of the "bipedal" Spring-loaded Inverted Pendulum (B-SLIP) in the presence of non-negligible damping. We first introduce an auxiliary system whose behavior under certain conditions is approximately equivalent to the B-SLIP in double-stance. Then, we derive approximate solutions to the dynamics of the new system following two different methods: (i) Updated-momentum approach that can deal with both the lossy and lossless B-SLIP models, and (ii) Perturbation-based approach following which we only derive a solution to the lossless case. The prediction performance of each method is characterized via a comprehensive numerical analysis. The derived representations are computationally very efficient compared to numerical integrations, and, hence, are suitable for online planning, increasing the autonomy of walking robots. Two application examples of walking gait control are presented. The proposed solutions can serve as instrumental tools in various fields such as control in legged robotics and human motion understanding in biomechanics.

Keywords: `Bio-Inspired Walking, Spring-Loaded Inverted Pendulum,`

*Corresponding author

[1]Delft Center for Systems and Control, Delft University of Technology, Mekelweg 2, 2628 CD Delft, The Netherlands. *Email address*: {m.shahbaziaghbelagh; r.babuska; g.a.delgadolopes}@tudelft.nl

[2]Department of Mechatronic Systems Engineering, Faculty of New Sciences and Technologies, University of Tehran, Tehran 14399-57131, Iran.

[3]Department of Computer Engineering, Middle East Technical University, Balgat 06531 Ankara, Turkey. *Email address*: saranli@ceng.metu.edu.tr

1. Introduction

Legged animals and humans are able to traverse most of the landmasses on the earth [1]. This unique mobility feature has attracted a large body of research both in biomechanics (to gain a better understanding of legged locomotion), and robotics (to design and control more efficient bio-inspired and bio-mimetic robots). The usefulness of such legged robots, hence, depends on the scientific and technological advances in those areas of research.

Understanding the underlying principles of legged locomotion that leads to the design, construction, and control of legged robots is challenging [2]. This is due to the complexities introduced by the intrinsic upright instability and the hybrid nature of legged locomotion. As such, researchers typically consider simplified (abstract) representations, that capture only the essential characteristics of the system under study. A noteworthy formal definition of this idea is the notion of *template* and *anchor* introduced by Full and Koditschek [3].

Following this definition, the Spring-loaded Inverted Pendulum (SLIP), which was first recognized in biomechanics as a good descriptive model of animals' hopping and running [4, 5], can be interpreted as a template for the running gait[6]. Starting with Raiberts' hoppers [1], which were based on an intuitive exploitation of SLIP behaviors, a number of dynamic robots have been introduced (e.g., [7, 8, 9, 10, 11]). Some of these robots were designed with no SLIP-like morphologies; however, they use SLIP as their target dynamics in the control calculations, extending the utility of SLIP to a broader scope.

Recently, Geyer et al. [12] studied the potential of describing the walking gait with compliant legs on the "bipedal" SLIP (B-SLIP) model. Contrary to the classical inverted pendulum, which is a widely-used template for the class of walkers that are referred to as limit cycle walking robots [13], the B-SLIP is able to model non-instantaneous double-stance (DS) phases. Moreover, the ground reaction forces produced in the B-SLIP are closer to the human data

reported in [12]. Subsequently, the idea of realizing dynamic walking has been studied both on the B-SLIP model itself [14, 15], and on more complex robot models through the embedding of B-SLIP behaviors [16, 17, 18, 19], showing the need for further investigations.

One potential benefit of designing a robot controller based on a template model such as SLIP is the ability to perform online planning. This is a crucial requirement for robust and reliable reactions of autonomous robots negotiating unexpected situations. Here, an analytical approach to the system dynamics seems useful since numerical integration of the equations of motion for most legged robots is not preferable due to its time-consuming nature[4]. Indeed, an (approximate) analytic solution of the SLIP dynamics is evaluated at least 250 times faster than the corresponding numerical solution, as discussed in [20]. An analytical approach could also be useful in analytically deriving the associated Jacobian matrix, which is an important tool for subsequent computations.

Unfortunately, it is known that the *exact* analytical time-domain solution to the SLIP equations of motion in the stance phase is not available. For the single-stance (SS) phase, however, a number of analytical approximations have been proposed [21, 22, 23, 24, 25, 26]. In particular, the method presented in [26], which is inspired by [23], can effectively represent the SLIP dynamics even in the presence of non-negligible damping. Recently, the effectiveness of this method has also been supported by an experimental validation in [27].

We have recently introduced the first approximation to the DS dynamics of the lossless B-SLIP model [28]. The predictive power of the proposed map was investigated through a numerical error analysis, corroborating its effectiveness. However, assuming such an ideal lossless model limits the direct application of the results to real robotic systems, in which energy dissipation via damping is inevitable. Moreover, although the proposed solution is computationally much

[4]Note that offline planners can also be used online through lookup tables. However, the effectiveness of this approach is limited to the precomputed values for the space of system states that may not cover unforeseen situations.

more efficient than numerical integration, it embodies a two-step iterative form, affecting its practicality for parametric analysis.

The main goal of the present study is to address these two issues. We derive a complete approximate solution to the DS dynamics of the lossy B-SLIP model, in which the effect of non-negligible damping is explicitly accounted for. At the core of the solution is the idea of approximating the B-SLIP trajectories in the DS phase (depicted in Figure 1a) by those of an auxiliary system, which we refer to as the lossy Axial-Torsional SLIP (AT-SLIP) (see Figure 1b). We determine conditions and parameter combinations under which the two systems are approximately equivalent. The significance of the AT-SLIP model is in its relatively simple structure that facilitates the process of approximation. When the two systems are approximately equivalent, any solution we derive to the AT-SLIP dynamics also qualifies as a solution to the B-SLIP dynamics in DS phase. In deriving the approximate solution to the lossy AT-SLIP dynamics, we are primarily motivated by the approach proposed in [23] and extended in [26], namely the Updated-momentum (UM) approach. However, substantial extensions have been made due to additional complexities introduced by the torsional spring and damper elements.

For the lossless DS phase, we revisited our previous results [28] by taking a different approach, namely the Perturbation-based (PB) approach, wherein we compute the approximations in a single step. Although the new approximations seem more complicated, they are suitable for functional analysis as there is no need for an extra iteration in the calculations. Nevertheless, both the previous two-step and the new single-step approximation methods yield sufficiently accurate predictions of system trajectories.

For both solutions, a careful characterization of the approximation errors is presented. The predictive power is assessed via an extensive numerical analysis, which simulates highly non-symmetric trajectories in the presence of non-negligible damping, with initial conditions that cover reasonable domains of the B-SLIP motion.

The obtained approximate solutions can be useful in various fields of study,

including planing and control for bio-inspired legged robots (see e.g., [18, 29, 30]). We finally present two controllers that leverage on the predictive power and analytic simplicity of the derived solutions. The simulation results show that the analytical approach taken in this study is instrumental in designing online planners, particularly necessary for autonomous robots.

2. The SLIP model and its derivatives

2.1. The B-SLIP model

The B-SLIP model in DS configuration is depicted in Figure 1a. The model represents a body with a point mass m located at the center of mass (CoM) connected to two compliant freely rotating massless legs, moving in the sagittal plane with gravitational acceleration g. The massless legs are endowed with linear stiffness k_0, viscous damping b_0, and rest length l_{rest}. The continuous state vector for this system is represented by $s := \begin{bmatrix} x & \dot{x} & y & \dot{y} \end{bmatrix}^T$, with $s \in \mathcal{S} \subset \mathbb{R}^4$. A discrete state vector is also considered as $q := \begin{bmatrix} x_{\text{h}}, x_{\text{f}}, \alpha, \mathcal{M} \end{bmatrix}^T$, where x_{h} and x_{f} are the hind and fore foot positions, respectively, α is the touchdown angle, and $\mathcal{M} \in \{\text{SS}, \text{DS}\}$. The last two variables of q will be used in Section 4, wherein a complete walking cycle is treated (see Figure 3).

The CoM equations of motion in DS in Cartesian coordinates (x, y) can be written as:

$$\begin{aligned} \begin{bmatrix} m\ddot{x} \\ m\ddot{y} \end{bmatrix} =& T_{\text{DS}}(s,q) \begin{bmatrix} k_0 \left(l_{\text{rest}} - l_{\text{f}}(s,q)\right) - b_0 \dot{l}_{\text{f}}(s,q) \\ k_0 \left(l_{\text{rest}} - l_{\text{h}}(s,q)\right) - b_0 \dot{l}_{\text{h}}(s,q) \end{bmatrix} \\ &+ \begin{bmatrix} 0 \\ -mg \end{bmatrix}, \end{aligned} \tag{1}$$

where l_{f} and l_{h} are the fore and hind leg length, respectively, and

$$T_{\text{DS}}(s,q) := \begin{bmatrix} -\sin\phi_{\text{f}}(s,q) & -\sin\phi_{\text{h}}(s,q) \\ \cos\phi_{\text{f}}(s,q) & \cos\phi_{\text{h}}(s,q) \end{bmatrix},$$

is a transformation matrix.

2.2. The AT-SLIP model

As depicted in Figure 1b, the AT-SLIP consists of the same mass, m, on top of a *single* leg with an axial stiffness k_{a} and damping b_{a}. The toe is affixed to the ground at the midpoint of the fore and hind toes. A torsional spring and damper is added to the toe, with spring constant k_{t} and viscous damping b_{t}. Denote by r_{rest} and θ_{rest} the rest length of the axial spring and the zero torque angle of the torsional spring, respectively.

The AT-SLIP CoM equations of motion in Cartesian coordinates (x, y) are as follows:

$$\begin{aligned}\begin{bmatrix} m\ddot{x} \\ m\ddot{y} \end{bmatrix} =& T_{\mathrm{AT}}(s,q) \begin{bmatrix} k_{\mathrm{a}}\left(r_{\mathrm{rest}} - r(s,q)\right) - b_{\mathrm{a}}\dot{r}(s,q) \\ \dfrac{k_{\mathrm{t}}\left(\theta_{\mathrm{rest}} - \theta(s,q)\right)}{r(s,q)} - \dfrac{b_{\mathrm{t}}\dot{\theta}(s,q)}{r(s,q)} \end{bmatrix} \\ &+ \begin{bmatrix} 0 \\ -mg \end{bmatrix}, \end{aligned} \tag{2}$$

where (r, θ) is a polar coordinates system, as defined in Figure 1b, and

$$T_{\mathrm{AT}}(s,q) := \begin{bmatrix} -\sin\theta(s,q) & \cos\theta(s,q) \\ \cos\theta(s,q) & \sin\theta(s,q) \end{bmatrix}.$$

2.3. Equivalence of models

The aim of this section is to find a set of parameters $(\theta_{\mathrm{rest}}, r_{\mathrm{rest}}, k_{\mathrm{a}}, k_{\mathrm{t}}, b_{\mathrm{a}}, b_{\mathrm{t}})$, as functions of the B-SLIP parameters, with which the AT-SLIP best approximates the B-SLIP in DS. To do so, we first assume that the motion of the CoM is such that it imposes the following conditions to the AT-SLIP states:

$$\frac{r_{\mathrm{rest}} - r}{r_{\mathrm{rest}}} \ll 1, \tag{3}$$

$$\cos\theta \approx 1. \tag{4}$$

Assumption (3) requires that the maximum compression of the axial spring is much smaller than its rest length. Assumption (4) implies that the angle spanned by the torsional spring is small with the axial spring predominantly

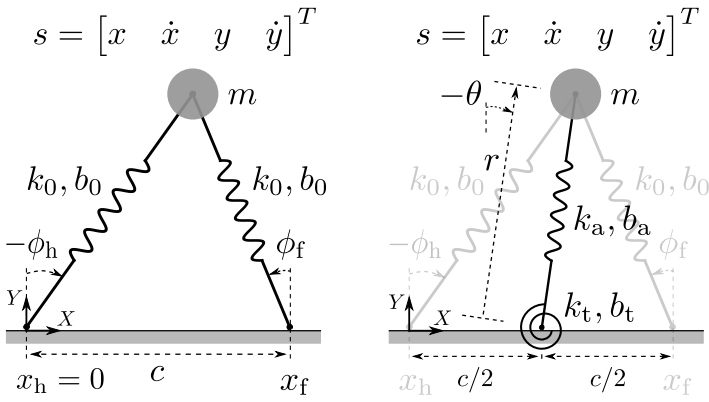

(a) B-SLIP (b) AT-SLIP

Figure 1: (a) The "bipedal" SLIP (B-SLIP) model depicted in the double-stance (DS) phase, and (b) the Axial-torsional SLIP (AT-SLIP) model, which approximates the CoM trajectories of the former system.

vertical. These assumptions largely remain valid for the normal range of motions of the SLIP system, and have been commonly made in the literature (see, for example, [23]).

When equivalent, the two systems exert the same resultant forces on the mass m for any arbitrary state (see Figure 2a). Moreover, the spring constants leading to the equivalency in the presence and absence of damping should be the same. This follows from the fact that the spring force is conservative whereas the damping force is dissipative. Taking this into account, in the rest of this section we propose a step by step procedure for relating the parameters of AT-SLIP to those of the B-SLIP.

According to Figure 2b, the zero spring force position of the B-SLIP is a symmetric configuration. For the chosen toe position illustrated in Figure 1b, this requires that

$$\theta_{\text{rest}} = 0. \tag{5}$$

Moreover, for the given configuration one can derive:

$$r_{\text{rest}} = \sqrt{l_{\text{rest}}^2 - c^2/4}. \tag{6}$$

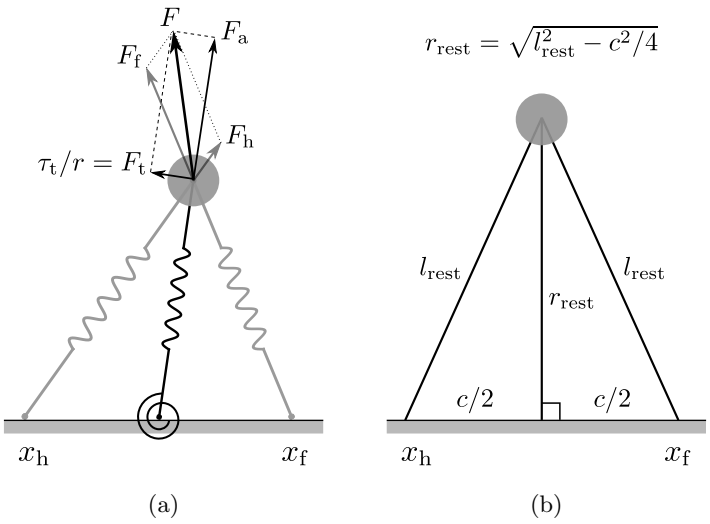

Figure 2: An illustration of the equivalency conditions between the B-SLIP and AT-SLIP models: (a) the springs force balance in an arbitrary configuration of the systems that is in accordance with assumptions (3) and (4), and (b) the zero spring force configuration of the two systems.

Next, we equate (1) to (2) while setting all damping coefficients to zero and solve the resulting relation for k_a and k_t to yield:

$$\begin{bmatrix} k_\mathrm{a}(s,q) \\ k_\mathrm{t}(s,q) \end{bmatrix} = A^{-1}(s,q) T_\mathrm{DS}(s,q) \begin{bmatrix} k_0 \left(l_\mathrm{rest} - l_\mathrm{f}(s,q)\right) \\ k_0 \left(l_\mathrm{rest} - l_\mathrm{h}(s,q)\right) \end{bmatrix}, \tag{7}$$

with

$$A(s,q) = T_\mathrm{AT}(s,q) \begin{bmatrix} r_\mathrm{rest} - r(s,q) & 0 \\ 0 & \dfrac{-\theta(s,q)}{r(s,q)} \end{bmatrix}.$$

It is clear that the resulting stiffnesses are functions of (x, y) and, hence, vary across the range of motion. However, numerical parameter estimation reveals that for the range of motion for which assumptions (3) and (4) remain largely valid, they can be approximated by specific limit values. To find a closed-form solution for the above observation, we compute the limit of $k_\mathrm{a}(s,q)$ and $k_\mathrm{t}(s,q)$

when x and y approach $c/2$ and r_{rest}, respectively:

$$k_{\text{a}} = \lim_{(x,y)\to(c/2,r_{\text{rest}})} k_{\text{a}}(s,q) = 2\left(r_{\text{rest}}/l_{\text{rest}}\right)^2 k_0, \tag{8}$$

$$k_{\text{t}} = \lim_{(x,y)\to(c/2,r_{\text{rest}})} k_{\text{t}}(s,q) = c^2/2\left(r_{\text{rest}}/l_{\text{rest}}\right)^2 k_0. \tag{9}$$

The resulting simple expressions also make intuitive sense. For instance, if $c \to 0$ then $r_{\text{rest}} \to l_{\text{rest}}$, thereby $k_{\text{a}} \to 2k_0$ and $k_{\text{t}} \to 0$.

Now that we have derived the expressions for k_{a} and k_{t}, we can equate (1) to (2), but this time in the presence of damping forces. By following a similar procedure as for the spring constants and in the sense of approximation, we eventually obtain:

$$b_{\text{a}} = 2\left(r_{\text{rest}}/l_{\text{rest}}\right)^2 b_0, \tag{10}$$

$$b_{\text{t}} = c^2/2\left(r_{\text{rest}}/l_{\text{rest}}\right)^2 b_0. \tag{11}$$

In summary, for the set $(\theta_{\text{rest}}, r_{\text{rest}}, k_{\text{a}}, k_{\text{t}}, b_{\text{a}}, b_{\text{t}})$ we derived expressions (5), (6), (8), (9), (10), (11), with which the AT-SLIP approximates the dynamics of the B-SLIP in DS, provided that assumptions (3) and (4) hold.

Note that in [28], for the case of lossless B-SLIP, we presented a different approach to find the equivalency relations. Although the obtained expressions for $k_{\text{a}}, k_{\text{t}}$ and r_{rest} are different from those derived here, they result in very similar numerical values.

3. Analytical solutions to the double-stance dynamics

In this section we present novel approximate solutions to the DS dynamics of both the lossy and lossless B-SLIP models. We address this open problem by solving, instead, the dynamics of the AT-SLIP model. As shown in the previous section, the resultant force exerted on the CoM of AT-SLIP and of B-SLIP in DS are approximately the same. Thereby, solving the equations of motion of the two systems results in approximately the same trajectories, when starting from the same initial conditions. We begin by deriving a complete solution for the lossy AT-SLIP and then focus on the special case of lossless system by taking two different approaches.

3.1. The Updated-momentum approach for the lossy AT-SLIP

The equations of motion of AT-SLIP in Cartesian coordinates (x, y) were derived in Section 2.2. Here, we transform them into polar coordinates (r, θ) for the sake of convenience, yielding:

$$m(\ddot{r} - r\dot{\theta}^2) = k_{\mathrm{a}}(r_{\mathrm{rest}} - r) - b_{\mathrm{a}}\dot{r} - mg\cos\theta, \tag{12}$$

$$\dot{p} = -k_{\mathrm{t}}\theta - b_{\mathrm{t}}\dot{\theta} + mgr\sin\theta, \tag{13}$$

where $p := mr^2\dot{\theta}$ is the angular momentum. The aim is to find a time domain solution for $r(t)$ and $\theta(t)$. The set of equations (12) and (13) represents a coupled nonlinear system of ODEs whose exact analytical solution is an open problem to date. To develop a workaround solution, we make assumptions (3) and (4), similar to the studies for the SS phase (see for example [23]), and seek a way to decouple the radial motion from the angular motion as follows.

3.1.1. Radial motion

Let us first apply assumption (4) in (12) and (13), leading to

$$m(\ddot{r} - r\dot{\theta}^2) = k_{\mathrm{a}}(r_{\mathrm{rest}} - r) - b_{\mathrm{a}}\dot{r} - mg, \tag{14}$$

$$\dot{p} = -b_{\mathrm{t}}\dot{\theta}. \tag{15}$$

Even this simplified version does not admit available analytical techniques. As such, we temporarily ignore the influence of torsional damping[5], resulting in the conservation of the angular momentum:

$$\dot{p} \approx 0, \tag{16}$$

thereby the angular momentum can be represented by its value at the initial condition (i.e., $p \approx p_0 := mr_0^2\dot{\theta}_0$). The corresponding angular velocity, $\dot{\theta} \approx p/(mr^2)$, is substituted into (14) to yield:

$$\ddot{r} + b_{\mathrm{a}}/m\dot{r} + k_{\mathrm{a}}/mr - p^2/(m^2r^3) = -g + k_{\mathrm{a}}/mr_{\mathrm{rest}}. \tag{17}$$

[5]We remedy the situation in Section 3.1.3 by reinforcing a correction on the angular momentum.

Still in this form, the equation contains the term $1/r^3$ which precludes the application of standard analytical tools. Following assumption (3) and similar to [23], we approximate this term using a Taylor series expansion:

$$1/r^3|_{r=r_{\text{rest}}} = 1/r_{\text{rest}}^3 - 3/r_{\text{rest}}^4(r - r_{\text{rest}}) + \dots. \tag{18}$$

Substituting the first two terms into (17) yields the following equation:

$$\ddot{r} + 2\xi\hat{\omega}_0\dot{r} + \hat{\omega}_0^2 r = F. \tag{19}$$

To keep the presentation concise, hereon all new parameters used in the derivations are defined in Appendix A, unless otherwise specified. The above equation is a linear inhomogeneous ODE whose solution, by setting the initial time to zero, can be determined as

$$r(t) = F/\hat{\omega}_0^2 + Me^{-\xi\hat{\omega}_0 t}\cos(\omega_{\text{d}} t + \phi). \tag{20}$$

Differentiation with respect to time yields the following relation for the radial velocity:

$$\dot{r}(t) = -M\hat{\omega}_0 e^{-\xi\hat{\omega}_0 t}\cos(\omega_{\text{d}} t + \phi + \phi_2). \tag{21}$$

3.1.2. Angular motion

For the angular motion, substitute $\dot{p} = mr^2\ddot{\theta} + 2mr\dot{r}\dot{\theta}$ into (15) and rearrange it to the following form:

$$\ddot{\theta}/\dot{\theta} = -2\dot{r}/r - b_{\text{t}}/(mr^2). \tag{22}$$

One can immediately take the integral over time from both sides:

$$\int \ddot{\theta}/\dot{\theta}\,\mathrm{d}t = -2\int \dot{r}/r\,\mathrm{d}t - b_{\text{t}}/m\int 1/r^2\,\mathrm{d}t + const. \tag{23}$$

The term $1/r^2$, with r as defined in (20), is approximated by a Taylor series expansion:

$$1/r^2|_{r=r_{\text{rest}}} = 1/r_{\text{rest}}^2 - 2/r_{\text{rest}}^3(r - r_{\text{rest}}) + \dots. \tag{24}$$

Substituting the first two terms into (23) and computing the integrals yields the following expression for the angular velocity:

$$\dot{\theta}(t) = z_0/r^2 e^{-\left(z_1 t + z_2 e^{(-\xi\hat{\omega}_0 t)}\cos(\omega_\mathrm{d} t + \phi - \phi_2)\right)}. \tag{25}$$

In order to derive a closed-form expression for $\theta(t)$, we need to compute the integral of $\dot{\theta}$ over time, which is not as simple. Here, we consider another approximation:

$$e^{(-\xi\hat{\omega}_0 t)}\cos(\omega_\mathrm{d} t + \phi - \phi_2) \approx z_3 t + z_4. \tag{26}$$

Applying this into (25) translates to:

$$\dot{\theta}(t) \approx z_0/r^2 e^{-(z_5 t + z_6)}. \tag{27}$$

Once again, we use an approximation of the term $1/r^2$ according to (24). Finally, integrating the resultant $\dot{\theta}$ over time yields[6]:

$$\theta(t) = \begin{cases} z_7 t + z_8 \sin(\omega_\mathrm{d} t + \phi) + z_9, & \text{if } b_\mathrm{t} = 0, \\ -z_7/z_5 e^{-(z_5 t + z_6)} + & \\ z_{10} e^{-(z_5 + \xi\hat{\omega}_0)t}\cos(\omega_\mathrm{d} t + \phi + \phi_3) + & \\ z_7/z_5 e^{-z_6} + z_{11}, & \text{otherwise.} \end{cases} \tag{28}$$

3.1.3. Necessary corrections

The reduced representations (14) and (15), used as a basis for the above approximations, are only valid when the DS trajectories are symmetric. This is only the case for steady-state walking. Even for this class of trajectories, the accuracy of the derived approximations can still be improved by a correction with respect to the total energy of the system.

[6]For b_t sufficiently close to zero, equation (28) results in invalid values, due to the presence of b_t in the denominators. According to our numerical analysis, this holds for $\xi_0 < 10^{-6}$, with $\xi_0 = b_0/(2\sqrt{k_0 m}) = b_\mathrm{t}/\left(c^2\sqrt{k_0 m}(r_\mathrm{rest}/l_\mathrm{rest})^2\right)$. However, for those values of ξ_0 one can safely ignore the effect of torsional damping by using the expression corresponding to $b_\mathrm{t} = 0$ condition.

To expand the domain of validity of our approximations to highly non-symmetric trajectories, we introduce two correction terms that compensate for the inaccuracies in the angular momentum: (i) the gravity-correction (denoted by p_{g}), inspired by [31]; (ii) a correction associated with the effect of torsional spring (denoted by p_{t}). The corrected angular momentum is computed as:

$$\hat{p} = p + p_{\mathrm{g}} + p_{\mathrm{t}}, \tag{29}$$

which replaces p in the corresponding derivations in our approximations, giving a two-iteration form to the UM method. The reset of this section presents the derivation of these correction terms.

The effect of gravitational force on the total angular momentum (p_{g}) can be approximately modeled as (see [31]):

$$p_{\mathrm{g}} = t_{\mathrm{e}} m g \bar{r} (\sin\theta_0 + \sin\theta_{\mathrm{e}})/2, \tag{30}$$

where $\bar{r}$ is the estimated average radial movement during the time interval from $t_0 = 0$ to t_{e}. This can be readily computed using (20):

$$\begin{aligned} \bar{r} &= 1/t_{\mathrm{e}} \int_0^{t_{\mathrm{e}}} r(t)\,\mathrm{d}t \\ &= F/\hat{\omega}_0^2 - M/(\hat{\omega}_0 t_{\mathrm{e}}) \left(z_4 - e^{-\xi\hat{\omega}_0 t_{\mathrm{e}}} \cos(\omega_{\mathrm{d}} t_{\mathrm{e}} + \phi - \phi_2)\right). \end{aligned} \tag{31}$$

An average effect of the torsional spring on the angular momentum can be computed as:

$$p_{\mathrm{t}} = \int_0^{t_{\mathrm{e}}} -k_{\mathrm{t}} \theta(t)\,\mathrm{d}t.$$

Substituting θ from (28) results in:

$$p_{\mathrm{t}} = \begin{cases} -k_{\mathrm{t}}(z_9 t_{\mathrm{e}} + z_7/2t_{\mathrm{e}}^2 - \\ z_8/\hat{\omega}_0(\cos(\hat{\omega}_0 t_{\mathrm{e}} + \phi) - \cos\phi)), & \text{if } b_{\mathrm{t}} = 0, \\ -k_{\mathrm{t}}\big(\big(z_7/z_5 e^{-z_6} + z_{11}\big)t_{\mathrm{e}} - \\ z_7/z_5^2 e^{-z_6}\big(1 - e^{-z_5 t_{\mathrm{e}}}\big) + \\ z_{12}\big(e^{-(z_5+\xi\hat{\omega}_0)t_{\mathrm{e}}} \cos(\omega_{\mathrm{d}} t_{\mathrm{e}} + \phi + 2\phi_3) \\ -\cos(\phi + 2\phi_3)\big)\big) & \text{otherwise.} \end{cases} \tag{32}$$

The derived p_{g} and p_{t} are substituted in (29) to give the corrected angular momentum $\hat{p}$, with which the corresponding derivations need to be repeated.

Once the improved approximations are determined, there is still the possibility to increase the accuracy by introducing a correction with respect to the system energy. To do so, we need to derive a closed-form solution for the energy losses due to damping.

The amount of energy losses due to the axial damping of the AT-SLIP can be expressed as:

$$E_{\mathrm{br}} = \int_0^{t_{\mathrm{e}}} b_{\mathrm{a}} \dot{r}^2 \, \mathrm{d}t. \tag{33}$$

Using the derived expression (21) for $\dot{r}$ and calculating the integral leads to the following simple expression:

$$\begin{aligned} E_{\mathrm{br}} =& e^{-2\xi\hat{\omega}_0 t_{\mathrm{e}}} \big(- z_{13} - z_{14} \cos^2(\omega_{\mathrm{d}} t + \phi + \phi_2) \\ &+ z_{15} \sin(2\omega_{\mathrm{d}} t + 2\phi + 2\phi_2) \big) + z_{16}. \end{aligned} \tag{34}$$

Similarly, one can obtain the following for the torsional damping of the AT-SLIP, by using (27) for $\dot{\theta}$:

$$\begin{aligned} E_{\mathrm{bt}} =& \int_0^{t_{\mathrm{e}}} b_{\mathrm{t}} \dot{\theta}^2 \, \mathrm{d}t \\ =& z_{17} \big(\cos(\omega_{\mathrm{d}} t_{\mathrm{e}} + \phi + \phi_4) e^{-(2z_5 + \xi\hat{\omega}_0)t_{\mathrm{e}}} - \\ & \cos(\phi + \phi_4) \big) + z_{18} \big(e^{-2z_5 t_{\mathrm{e}}} - 1 \big). \end{aligned} \tag{35}$$

Now, $E_{\mathrm{b}} = E_{\mathrm{br}} + E_{\mathrm{bt}}$ accounts for the total energy losses of the AT-SLIP, which also gives an approximation of the energy lost in the DS phase of B-SLIP motion. Subsequently, this can be used to compute a corrected angular velocity at the end of DS phase (i.e., the liftoff state):

$$\hat{\dot{\theta}}_{\mathrm{e}} = \mathrm{sgn}(\dot{\theta}_{\mathrm{e}}) \sqrt{|2/m(E_0 - V_{\mathrm{e}} - E_{\mathrm{b}}) - \dot{r}_{\mathrm{e}}^2|} / r_{\mathrm{e}}, \tag{36}$$

where E_0 and V_{e} are best obtained from the original B-SLIP model:

$$\begin{aligned} E_0 =& 1/2m\big(\dot{x}_0^2 + \dot{y}_0^2\big) + 1/2k_0(l_{\mathrm{rest}} - l_{\mathrm{f0}})^2 \\ &+ 1/2k_0(l_{\mathrm{rest}} - l_{\mathrm{h0}})^2 + mgy_0, \end{aligned} \tag{37}$$

$$V_{\mathrm{e}} = 1/2k_0(l_{\mathrm{rest}} - l_{\mathrm{fe}})^2 + 1/2k_0(l_{\mathrm{rest}} - l_{\mathrm{he}})^2 + mgy_{\mathrm{e}}, \tag{38}$$

with l_{i0} and l_{ie}, $i \in \{\mathrm{f}, \mathrm{h}\}$, are the legs' length at the initial (i.e., fore leg touchdown) and the end (i.e., hind leg liftoff) states, respectively.

This completes the approximate solution proposed in this study to the dynamics of AT-SLIP system, which also qualifies as a solution to the DS dynamics of the lossy B-SLIP from any initial to any end states, including the touchdown to liftoff map. The accuracy of the presented approximations will be assessed in Section 5.

3.2. The Perturbation-based approach for the lossless AT-SLIP

The UM method, presented in the previous section, effectively approximates the dynamics of both lossy and lossless AT-SLIP models. In this section, we propose a different approach to approximate the *lossless* AT-SLIP which, thanks to the available tools in perturbation theory, features a straightforward form. From the perspective of functional analysis, this is generally more effective than the UM method, in which the derivations need to be repeated once using the updated angular momentum.

Inspired by the study on the approximation of the SS map [25] and different from the previous method, we assume that the angular momentum is only conserved for the radial motion and not for the angular motion. Consequently, the radial motion equation is solved similarly to the previous method to yield the following relation:

$$r(t) = F/\hat{\omega}_0^2 + M\cos(\hat{\omega}_0 t + \phi), \tag{39}$$

For the angular motion, we start by substituting

$$\theta(t) = \nu(t)u(t) \tag{40}$$

into (13), with $\sin\theta \approx \theta$ and $b_{\mathrm{t}} = 0$ (because of the lossless case). This will help us to translate the equation into the form suitable for perturbation techniques. The resulting relation becomes:

$$\begin{aligned} \ddot{u} + (2\dot{\nu}/\nu + 2\dot{r}/r)\dot{u} + (\ddot{\nu}/\nu + 2\dot{r}\dot{\nu}/(r\nu) - g/r + \\ k_{\mathrm{t}}/(mr^2))u = 0. \end{aligned} \tag{41}$$

To be able to use the perturbation based solution, we choose ν such that the first derivative of u disappears:

$$2\dot{\nu}/\nu + 2\dot{r}/r = 0. \tag{42}$$

It is clear that $\nu = 1/r$ solves this equation. Substituting this into (41) yields the following relation between u and its second derivative:

$$\ddot{u} - (-\hat{\omega}_0^2 + \frac{F+g}{r} - \frac{k_\mathrm{t}/m}{r^2})u = 0. \tag{43}$$

To solve this equation analytically, we need to approximate the terms $1/r$ and $1/r^2$ with r as defined in (39). By defining $\varepsilon := \frac{M}{F/\hat{\omega}_0^2}$ and taking into consideration that ε remains close to zero (according to assumption (3)), one can obtain the following approximations:

$$\frac{1}{r} \approx \frac{1}{F/\hat{\omega}_0^2} - \frac{1}{F/\hat{\omega}_0^2}\varepsilon\cos(\hat{\omega}_0 t + \phi), \tag{44}$$

$$\frac{1}{r^2} \approx (\frac{1}{F/\hat{\omega}_0^2})^2 - 2(\frac{1}{F/\hat{\omega}_0^2})^2\varepsilon\cos(\hat{\omega}_0 t + \phi). \tag{45}$$

Applying these approximations in (43) translates to the following form:

$$\ddot{u} - (\mu - \varepsilon\delta\cos(\hat{\omega}_0 t + \phi))\, u = 0, \tag{46}$$

where:

$$\mu := \frac{1}{F/\hat{\omega}_0^2}\left(g - \frac{k_\mathrm{t}/m}{F/\hat{\omega}_0^2}\right), \tag{47}$$

$$\delta := \mu + \frac{1}{F/\hat{\omega}_0^2}\left(F - \frac{k_\mathrm{t}/m}{F/\hat{\omega}_0^2}\right). \tag{48}$$

Since it is assumed that ε remains close to zero, one can derive an analytical approximation for this equation using standard perturbation techniques. The solution is a power series in terms of ε:

$$u(t) = u_0(t) + \varepsilon u_1(t) + \varepsilon^2 u_2(t) + \cdots \tag{49}$$

Substituting this into (46) and balancing the terms with the same power of ε yields a series of linear time-invariant ODEs. We approximate the solution by

only the first-order expansion:

$$\varepsilon^0: \quad \ddot{u}_0 - \mu u_0 = 0, \quad u_0(0) = u(0), \dot{u}_0(0) = \dot{u}(0), \tag{50}$$

$$\varepsilon^1: \quad \ddot{u}_1 - \mu u_1 = -\delta u_0 \cos(\hat{\omega}_0 t + \phi), \tag{51}$$

$$u_1(0) = 0, \dot{u}_1(0) = 0.$$

Depending on the value of μ different conditions are possible:

- If $\mu > 0$:

Define $\lambda^2 = \mu$, and solve (50) to yield:

$$u_0(t) = c_1 e^{\lambda t} + c_2 e^{-\lambda t}. \tag{52}$$

The parameters c_1 and c_2 are determined by the initial conditions given in (50). Having the solution of u_0, one can solve (51):

$$\begin{aligned} u_1(t) = {} & c_3 e^{\lambda t} + c_4 e^{-\lambda t} \\ & + \frac{c_1 \delta}{4\lambda^2 + \hat{\omega}_0^2} e^{\lambda t} \left(\cos(\hat{\omega}_0 t + \phi) - \frac{2\lambda}{\hat{\omega}_0} \sin(\hat{\omega}_0 t + \phi) \right) \\ & + \frac{c_2 \delta}{4\lambda^2 + \hat{\omega}_0^2} e^{-\lambda t} \left(\cos(\hat{\omega}_0 t + \phi) + \frac{2\lambda}{\hat{\omega}_0} \sin(\hat{\omega}_0 t + \phi) \right). \end{aligned} \tag{53}$$

Similarly, c_3 and c_4 are determined by the initial conditions specified in (51).

- If $\mu < 0$ and $\mu \neq -\hat{\omega}_0^2/4$:

By defining $\lambda^2 = -\mu$, and following the similar procedure as before:

$$\begin{aligned} u_0(t) = {} & c_1 \sin(\lambda t) + c_2 \cos(\lambda t), \\ u_1(t) = {} & c_3 \sin(\lambda t) + c_4 \cos(\lambda t) \\ & + \frac{N\delta}{4\lambda^2 - \hat{\omega}_0^2} \left(-\frac{2\lambda}{\hat{\omega}_0} \sin(\hat{\omega}_0 t + \phi) \sin(\lambda t + \psi) \right. \\ & \left. - \cos(\hat{\omega}_0 t + \phi) \cos(\lambda t + \psi) \right), \end{aligned} \tag{54}$$

where $N := \sqrt{c_1^2 + c_2^2}$, and $\psi := \arctan(-c_1/c_2)$. For the solution of u_0 and u_1 in especial cases $\mu = -\hat{\omega}_0^2/4$ and $\mu = 0$ please see Appendix B.

Once u_0 and u_1 are computed, then the time domain solution of θ can be written as:

$$\theta(t) = u(t)\nu(t) = \frac{u_0(t) + \varepsilon u_1(t)}{r(t)}. \tag{55}$$

Equations (39) and (55) are closed-form relations that approximate the dynamics of the AT-SLIP, and hence the DS dynamics of the lossless B-SLIP, in a single-iteration form. A final energy-based correction on the angular velocity at the end of motion will additionally increase the prediction accuracy, by following a similar procedure presented in Section 3.1.3.

Concerning the lossy AT-SLIP, while the solution of ν would not be as simple, the subsequent derivations require more algebraic computations and additional simplifications. For this class of problems, we hence conclude that the proposed UM approach suits better.

4. The whole walking cycle

The bipedal walking gait is the composition of alternating SS and DS phases of the B-SLIP model. In the present study, we have developed an analytical approximate time domain solution for the DS dynamics of the system in the presence of non-negligible damping. For a similar solution to the SS dynamics please refer to [26].

A complete walking step can be characterized as illustrated in Figure 3. The vertical leg orientation (VLO) defines the start of a step. The system transitions from the first SS to DS phase by the *touchdown* event, when the fully stretched swing leg touches the ground with touchdown angle α. The touchdown instant therefore solves the following equation:

$$l_{\mathrm{h}}(t_{\mathrm{t}}) \cos \phi_{\mathrm{h}}(t_{\mathrm{t}}) - l_{\mathrm{rest}} \sin \alpha = 0. \tag{56}$$

The system transitions back to the SS phase by the *liftoff* event, when the ground reaction force of the hind leg reduces to zero during decompression. Mathematically speaking:

$$k_0 \left(l_{\mathrm{rest}} - l_{\mathrm{h}}(t_{\mathrm{l}})\right) - b_0 \dot{l}_{\mathrm{h}}(t_{\mathrm{l}}) = 0. \tag{57}$$

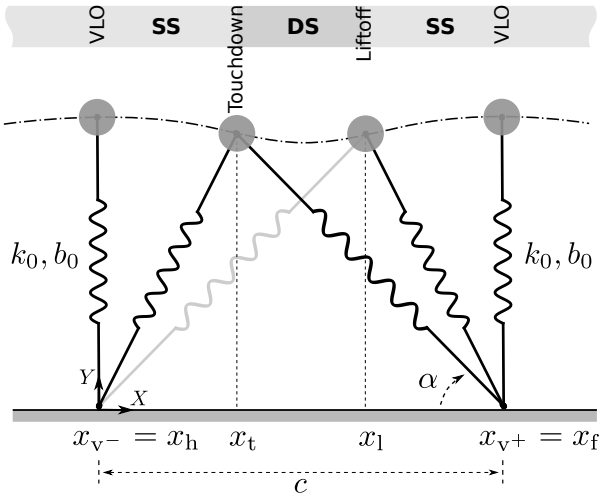

Figure 3: A complete step of walking gait for the B-SLIP model.

Notice that in case of lossless B-SLIP, (57) will reduce to $l_{\mathrm{h}}(t_{\mathrm{l}}) - l_{\mathrm{rest}} = 0$ (i.e., the system lifts off when the hind leg is fully stretched).

Solving (56) and (57) for the touchdown and liftoff instances analytically is challenging, even by applying the derived approximations. However, one can solve these transition equations numerically, and the resulting solutions are feasible owing to the one-dimensional and monotonic nature of the equations.

For the system depicted in Figure 3, every trajectory which is mirrored about the vertical passing $x = c/2$ is symmetric. It can be shown that for a symmetric DS of lossless B-SLIP, the correction terms (30) and (32) are naturally reduced to zero. Therefore, for this class of trajectories, the equivalent AT-SLIP model does not need the torsional spring, if the prediction of liftoff state (namely, the DS map) is desired. This means that the symmetric DS trajectories of the lossless B-SLIP can be approximated by the trajectories of a *monopedal* SLIP model endowed with certain parameters, as shown in Figure 4. This highlights the merits of the equivalency conditions achieved in this study.

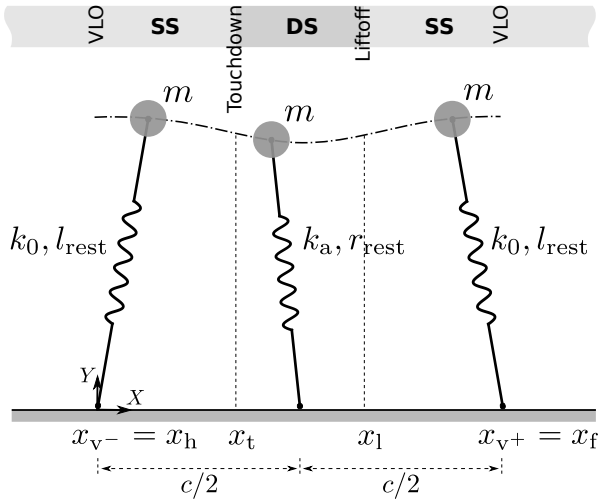

Figure 4: A symmetric lossless walking step can be approximated by the composition of "three SS phases". Note that $k_{\text{a}} = 2\,(r_{\text{rest}}/l_{\text{rest}})^2\,k_0$, and $r_{\text{rest}} = \sqrt{l_{\text{rest}}^2 - c^2/4}$.

5. Characterization of approximation errors

In this section, we investigate the performance of the proposed approximations by quantifying the prediction errors. First, the predicted liftoff states by our approximations, both for the lossless and lossy SLIP models in DS, are compared to the "ground truth" data, obtained via numerical integration of the original B-SLIP model. Then, we consider a whole walking step and assess the associated errors, which are contributed by both SS and DS approximations.

5.1. Simulation setting and performance criteria

The "ground truth" data are obtained using a hybrid solver that we have developed in Python 2.7 using the standard available modules. The solver is equipped with a variable step size integrator that captures the switching between phases, governed by (56) and (57), precisely. This solver, together with the associated approximate maps, can be accessed online [32].

The simulation covers a set of most feasible locomotion properties, by spanning five dimensions: the horizontal velocity at VLO ($\dot{x}_{\text{v}}$), the height at VLO

(y_{v}), the legs stiffness (k_0), the "relative" touchdown angle (α_{rel})[7], and the damping ratio defined as $\xi_0 := b_0/(2\sqrt{mk_0})$. Table 1 gives the variation domains of these initial conditions and system parameters. Without loss of generality, we set $m = 80\,\mathrm{kg}$ and $l_{\mathrm{rest}} = 1\,\mathrm{m}$ similarly to average human data, and we assume the vertical velocity at starting VLO ($\dot{y}_{\mathrm{v}}$) is zero.

A simulation is considered valid if (i) the system accomplishes one complete step of walking, and (ii) it is possible for the system to further touch down for the next step. To satisfy the first condition, trials in which the CoM hits the ground or moves backward, or when the system completely leaves the ground (airborne phase), are not stored. Concerning the second condition, denote by E_{min} the minimum amount of the mechanical energy at VLO required to make the next touchdown:

$$E_{\mathrm{min}} = mgl_{\mathrm{rest}} \sin\alpha + 1/2k_0 l_{\mathrm{rest}}^2 (1 - \sin\alpha)^2.$$

Then, the total energy at the starting VLO, E_{v}, should satisfy the following property:

$$E_{\mathrm{v}} \geq E_{\mathrm{min}}.$$

Parameter combinations resulting in E_{v} that violate this property are excluded. The total number of 70,117 runs satisfied the first condition, out of which 55,593 runs also satisfied the second condition.

To investigate the predictive performance, we use the following percentage error measures in different system states:

$$e_{\mathrm{p}} := 100 \frac{||(x,y)_{\mathrm{true}} - (x,y)_{\mathrm{approx}}||_2}{||(x,y)_{\mathrm{true}}||_2}, \tag{58}$$

$$e_{\dot{\mathrm{p}}} := 100 \frac{||(\dot{x},\dot{y})_{\mathrm{true}} - (\dot{x},\dot{y})_{\mathrm{approx}}||_2}{(||(\dot{x},\dot{y})_{\mathrm{true}}||_2)_{\mathrm{max}} - (||(\dot{x},\dot{y})_{\mathrm{true}}||_2)_{\mathrm{min}}}, \tag{59}$$

$$e_{\mathrm{E}} := 100 \frac{|E_{\mathrm{true}} - E_{\mathrm{approx}}|}{E_{\mathrm{true}}}, \tag{60}$$

[7]Similarly to [26], the relative touchdown angle is defined as: $\alpha_{\mathrm{rel}} := \alpha - \alpha_{\mathrm{n}}$, with α_{n} being the *neutral* touchdown angle [33] resulting in a symmetric trajectory, for given initial state and system parameters.

Table 1: Initial conditions and system parameters spanned during the simulation

$y_{\mathrm{v}}(\mathrm{m})$	$\dot{x}_{\mathrm{v}}(\mathrm{m/s})$	$k_0(\mathrm{kN/m})$	α_{rel}	ξ_0
$\left[l_{\mathrm{rest}} \sin\alpha, l_{\mathrm{rest}}\right]$	$\left[0.5, 2\right]$	$\left[10, 40\right]$	$\left[-0.15, 0.15\right]$	$\left[0, 0.4\right]$

which evaluate percentage normalized errors associated with position, velocity and total energy, respectively. When the predictive performance of the DS or the whole walking step is under the investigation, these measures are evaluated at the liftoff or VLO states, respectively. Notice that $e_{\dot{\mathrm{p}}}$, by definition, remains practical even when the norm of true velocity ($||(\dot{x}, \dot{y})_{\mathrm{true}}||_2$) approaches zero, as the "min" and "max" norms are obtained from the entire range of simulation.

5.2. Performance of the lossless double-stance map

For the lossless B-SLIP model in DS, we have presented two different solutions following the UM and PB approaches in Section 3.1 and 3.2, respectively. To analyze the liftoff prediction errors, we provide both methods with the touchdown states of the ground truth data as the initial conditions.

The mean, standard deviation and maximum values of the resulting normalized errors are listed in the left part of Table 2. As can be seen, the liftoff states predicted by the PB approach are slightly more accurate than those of the UM approach. This can also be seen in Figure 5, in which the sum of the mean position and velocity errors ($e_{\mathrm{p}} + e_{\dot{\mathrm{p}}}$) are plotted with respect to the relative touchdown angle (α_{rel}). While the UM solution errors increase for larger negative α_{rel}, the PB errors are almost uniform. Overall, both methods succeed in accurately approximating the dynamics of the original system for the purpose of control design. This will be demonstrated in the next section where controllers designed based on these approximations are presented.

5.3. Performance of the lossy double-stance map

In the presence of damping, the UM approach described in Section 3.1 is applicable. The corresponding numerical errors are reported in Table 2 and

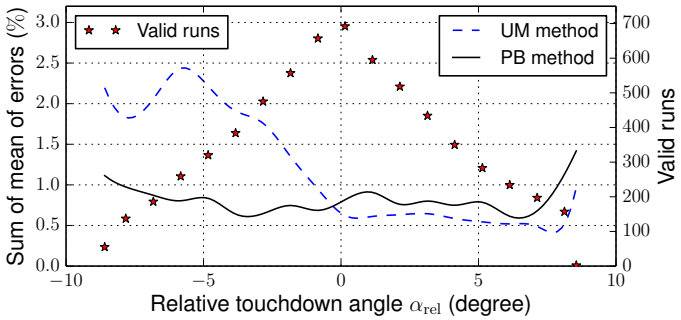

Figure 5: Lossless double-stance prediction errors are plotted versus the relative touchdown angle. For each bin, the number of valid runs, satisfying the requirements described in Section 5.1, are given in the right axis.

Table 2: Summary of the percentage prediction errors analysis, covering both the UM and PB methods for the lossless and lossy SLIP models.

	Double-stance phase									Whole walking cycle		
	Lossless						Lossy					
	PB method			UM method								
	mean	sd	max	mean	sd	max	mean	sd	max	mean	sd	max
e_{p} (%)	0.17	0.78	22.36	0.27	0.37	13.21	0.47	0.58	13.21	0.71	0.67	17.59
$e_{\dot{\text{p}}}$ (%)	0.61	1.09	35.15	0.83	1.39	31.17	1.56	1.79	28.45	1.05	1.62	22.86
e_{E} (%)	0	0	0	0	0	0	2.92	1.50	11.97	0.06	0.10	8.85

plotted with respect to the damping ratio in Figure 6. The error measures slightly increase for high damping ratios. This can mainly be due to the additional simplification (26) that negatively affects the derivation of both angular position (28) and the energy losses due to torsional damping (35).

5.4. Performance of the whole walking step

We now consider the composition of SS and DS phases which form a complete walking step, and investigate the predictive performance using the UM method. The corresponding normalized errors at VLO state are listed in the right part of Table 2. Note that from a control design point of view, the magnitude of

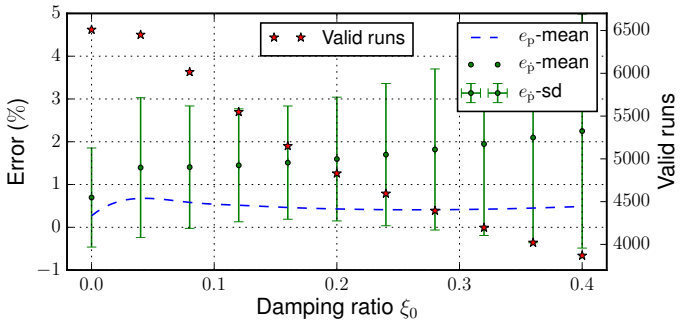

Figure 6: Lossy double-stance prediction errors are plotted versus the damping ratio. For each bin, the number of valid runs, satisfying the requirements described in Section 5.1, are given in the right axis.

these errors are important since they reflect the accuracy of the so called *VLO return map*, which serves as the basis of the control policies presented in the next section.

The normalized position and velocity errors are depicted in Figure 7 with respect to the damping ratio. There is no considerable change in the prediction performance when damping is introduced, and the method effectively handles the presence of a rather large damping. As can be seen in Figure 7a, the predicted VLO positions are even slightly more accurate for higher damping ratios, owing to the resulting smaller leg compressions satisfying assumption (3). The dependence of the prediction errors on the maximum relative leg compression, defined as $(r_{\mathrm{rest}} - r_{\mathrm{min}})/r_{\mathrm{rest}}$, is depicted in Figure 8.

6. Application to gait synthesis

6.1. Controlled passive walking on the lossless SLIP model

In this section we present a control application utilizing the predictive power of the PB solution proposed in Section 3.2. We start by the observation that the total energy of the system is invariant to the touchdown angle, since we assume no physical meaning for the swing leg. As such, modulating the touchdown angle to induce desired behaviors still results in a passive system. The corresponding control policy can be written as:

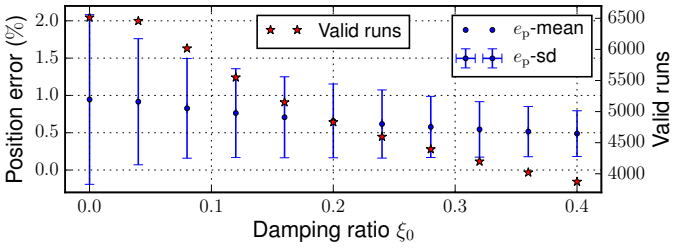

(a) Position errors

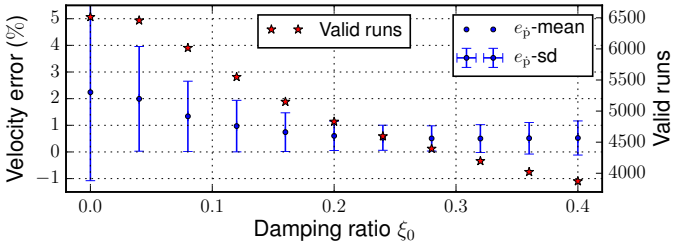

(b) Velocity errors

Figure 7: Approximate VLO return map errors are plotted versus the damping ratio. For each bin, the number of valid runs, satisfying the requirements described in Section 5.1, are given in the right axis.

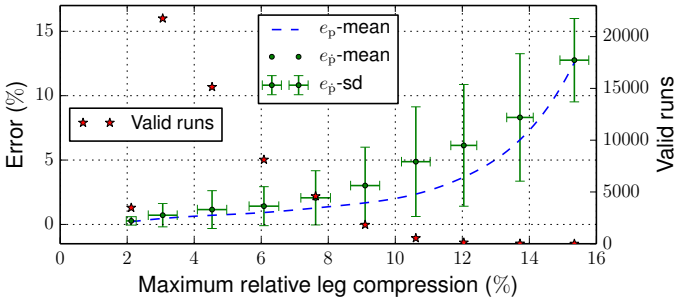

Figure 8: The dependence of the prediction errors on the maximum relative leg compression, defined as $(r_{\mathrm{rest}} - r_{\mathrm{min}})/r_{\mathrm{rest}}$, is shown. For each bin, the number of valid runs, satisfying the requirements described in Section 5.1, are given in the right axis.

$$\alpha = \underset{65^{\circ} \leq \alpha < 90^{\circ}}{\operatorname{argmin}} \; ||\tilde{s}^{*}_{\mathrm{v}+} - \mathcal{P}(\tilde{s}_{\mathrm{v}-})||, \tag{61}$$

where $\tilde{s}_{\mathrm{v}-}$ is the reduced state vector at a Poincaré section taken at VLO (that is the state vector s excluding the horizontal position x), $\tilde{s}^*_{\mathrm{v}+}$ is the desired (reduced) state vector at the next return in Poincaré section, and $\mathcal{P}(\cdot)$ is the associated return map built using the proposed PB solution. Note that we simply use the initial state as the desired state. Finally, the optimization (61) is run at each VLO to give the touchdown angle for the next step.

Figure 9a summarizes the simulation results for the system with $m = 80\,\mathrm{kg}, k_0 = 16.5\,\mathrm{kN/m}$ and $l_{\mathrm{rest}} = 1\,\mathrm{m}$. The dashed lines depict the domain of initial conditions, with no vertical velocity, that belong to particular energy levels. The dotted lines represent subsets of this domain for which there is at least one (fixed) touchdown angle leading to a stable walking gait in the uncontrolled SLIP[8]. Similarly, the initial conditions belonging in the solid lines form the domain of stable walking in the controlled SLIP system that is governed by the control policy (61). Note that running a sufficiently refined set of simulations would yield the aforementioned domains in the form of areas rather than the sets of points. However, such an extensive numerical study is beyond the scope of this paper.

For the investigated energy levels, the controlled system achieves a larger domain of stability compared to the uncontrolled SLIP. This is worthwhile since the controlled system does not require extensive numerical search for the proper touchdown angle a priori. However, for relatively high energy levels, especially when the initial height is close to the rest length, the presence of the considered controller does not yield noticeable improvements. Here it seems that the approximation error propagated in the control calculation is so that the system experiences undesired transitions to the flight phase, or prevents foot protraction. Nevertheless, selection of a different desired state for the mentioned domains can still grant stable walking for the controlled system, as revealed in our investigations.

[8]The angle is spanned from 65° to 90° with the delta increment 0.1°, and the gait is assumed stable if it can perform at least 50 steps in a row.

Finally, Figure 9b compares the CoM trajectories of the uncontrolled and controlled SLIP, starting with the initial condition of example point A given in Figure 9a. While the maximum number of steps that can be produced in the uncontrolled system occurs when the constant touchdown angle $\alpha = 76.1^{\circ}$ is used (14 steps), the controlled system produces stable walking. The control parameter, i.e., the varying touchdown angle, is depicted as well.

6.2. Energy-regulated walking on the lossy SLIP model

In this section, we demonstrate the utility of the UM approach (presented in Section 3.1) for the lossy B-SLIP through a control application. In the presence of non-negligible damping, it is clear that neither the uncontrolled SLIP nor the controlled passive SLIP (through modulation of the touchdown angle) can exhibit stable walking, due to the energy dissipation. Here, we devise a simple updating mechanism for the leg stiffness, relying on the proposed approximations, that regulates the system energy in a step-to-step manner.

Consider a walking step starting at VLO with the initial state vector $s_0 = \left[0, \dot{x}_{\mathrm{v}0}, y_{\mathrm{v}0}, 0\right]^T$, and the associated total energy $E_{\mathrm{v}0} = 1/2m\dot{x}_{\mathrm{v}0}^2 + 1/2k_0(l_{\mathrm{rest}} - y_{\mathrm{v}0})^2 + mgy_{\mathrm{v}0}$. To compensate for damping losses, we update the magnitude of stiffness once per step at the so called "virtual" bottom, where the distance between the mass and the mid-stance of the feet is minimum. The choice of virtual bottom is motivated by the fact that it is indeed the real bottom of the axial spring in the corresponding AT-SLIP model. The amount of energy dissipated from the starting VLO till the virtual bottom can readily be computed. For the rest of motion till the next VLO, however, we should predict the energy that will be dissipated. For that, we construct the map $\mathcal{H}(\cdot)$ that maps the states at virtual bottom s_{b} onto the states at the next VLO s_{v}, i.e.,

$$s_{\mathrm{v}} = \mathcal{H}(s_{\mathrm{b}}). \tag{62}$$

Note that $\mathcal{H}(\cdot)$ is the composition of two submaps: the virtual bottom to liftoff map in the DS phase and the liftoff to the next VLO map in the SS phase, which are constructed using the UM approximations. The total energy at the

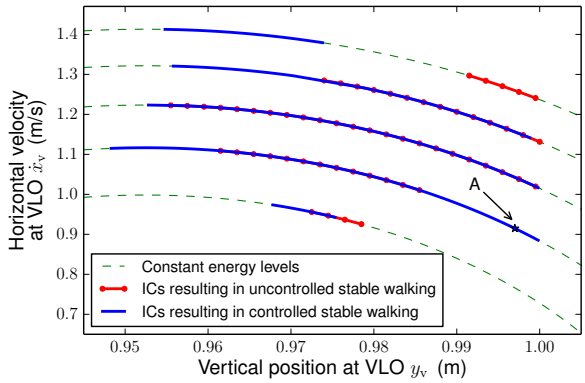

(a) Comparison of the domain of initial conditions resulting in stable walking gaits in the uncontrolled and controlled systems. The arbitrary chosen amount of energy levels from bottom to top are as follows: $\{806, 816, 826, 836, 846\}$, all are in Joule.

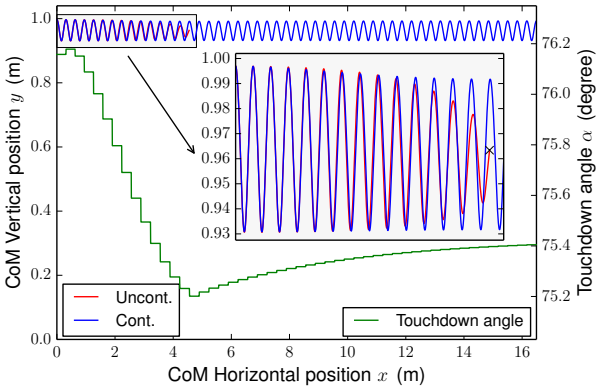

(b) CoM trajectories for the uncontrolled and controlled systems, starting with the initial condition of example point A. The control parameter (touchdown angle α) is plotted as well.

Figure 9: Simulation of a controlled SLIP model demonstrating the practical utility of the proposed DS map.

next VLO is then calculated using the predicted state s_v as $E_v = 1/2m(\dot{x}_v^2 + \dot{y}_v^2) + 1/2k_0(l_{rest} - y_v)^2 + mgy_v$. Finally, the legs' stiffness are updated at the

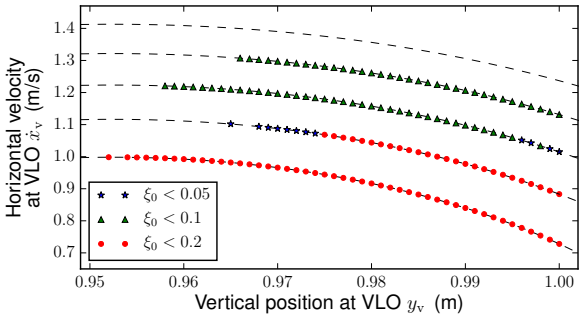

Figure 10: Domain of initial conditions resulting in stable walking gaits in the stiffness controlled lossy B-SLIP model. The arbitrary chosen amount of energy levels from bottom to top are as follows: $\{806, 816, 826, 836, 846\}$, all are in Joule. Different colors (and markers) indicate the largest damping ratio the system can handle.

virtual bottom according to the following relation:

$$k_0' = k_0 + 2(E_{\mathrm{v}0} - E_{\mathrm{v}})/\big((l_{\mathrm{rest}} - l_{\mathrm{bh}})^2 + (l_{\mathrm{rest}} - l_{\mathrm{bf}})^2\big), \tag{63}$$

where l_{bf} and l_{bh} are the legs' length at virtual bottom.

We have applied this energy regulation mechanism to the SLIP model used in the previous section with the same settings but in the presence of damping (with the damping ratio taking various values: $\xi_0 = \{0.05, 0.1, 0.2,\ 0.4\}$). Figure 10 shows the resulting domain of initial conditions leading to stable walking, even in the presence of non-negligible damping. Different colors indicate the largest damping value the system can handle (see the figure caption for a detailed description).

As can be seen, using the simple updating mechanism proposed, it is possible to perform stable walking gait still in the presence of damping, with comparatively large domain of attraction. Notice that, here again, the controller does not yield good results for very high energy levels for the same reason discussed in the previous application. However, for relatively low energy levels, the proposed control policy significantly enlarges the domain of initial conditions leading to stable walking, compared to the lossless passive system whose results was depicted in Figure 9a.

7. Conclusion

Analytic approximations of the otherwise non-integrable double-stance dynamics of the dissipative Spring-loaded Inverted Pendulum model have been studied in this paper. We have taken two different approaches, one focusing on the inclusion of an explicit effect of damping (the UM method), while the other is intended to yield a closed-form solution (the PB method). At the core of both methods is the approximation of the original bipedal SLIP trajectories by those of an auxiliary system referred to as the Axial-Torsional SLIP. We derived a simple approximate mapping between the parameters of the two systems, which under certain conditions enables the AT-SLIP to accurately approximate the original SLIP in double-stance.

Assessed through a comprehensive numerical investigation, covering highly non-symmetric trajectories with considerable amounts of damping, both methods provided accurate approximations of the original system dynamics. Due to strong coupling in the SLIP equations of motion in double-stance, the study of these dynamics is significantly more complicated than the single-stance dynamics. However, we have achieved almost the same accuracy compared to the existing solutions to the single-stance dynamics. Furthermore, for the especial case of lossless SLIP model (with no damping), we presented two distinct methods, which yield almost the same predictive performance, indicating the feasibility of the approaches taken. As an additional demonstration, we presented control applications exploiting the predictive power of the proposed methods, which thanks to the simplicity resulted from the analytical nature of the solutions, are suitable for online implementations.

The analytical perspective taken in this study opens avenues for tailoring the existing models in understanding humans and animals gaits in biomechanics, and for enhancing online planning and control methods for legged locomotion with non-instantaneous double-stance phases in robotics. The presented method can intuitively be extended to model the three-dimensional B-SLIP system, which has recently attracted significant interest in the field of dynamic

walking, by incorporating another torsional spring and damper. Currently, we are developing a framework to systematically designing control systems that exploit the presented results as target dynamics for real robotic walkers.

Appendix A. Parameters defined in the presentation of UM method in Section 3.1

Please see Table A.3 for the definition of the parameters used in the UM method. Also provided is the reference to the equation in which the defined parameter is used for the first time.

Appendix B. Details on derivations presented in Section 3.2

In this section, we present the time-domain solutions of u_0 and u_1 for two special cases:

- if $\mu = -\hat{\omega}_0^2/4$:

$$
\begin{aligned}
u_0(t) =& c_1 \sin(\lambda t) + c_2 \cos(\lambda t), \\
u_1(t) =& c_3 \sin\left(\frac{\hat{\omega}_0 t}{2}\right) + c_4 \cos\left(\frac{\hat{\omega}_0 t}{2} +\right) \\
& \frac{N\delta}{8\hat{\omega}_0^2 \sin\left(\frac{\hat{\omega}_0 t}{2}\right)} \left(-4\sin(\hat{\omega}_0 t - \phi + \psi) + \right. \\
& 2\hat{\omega}_0 t(\cos(\hat{\omega}_0 t + \phi - \psi) - \cos(\phi - \psi)) + \\
& \sin(2\hat{\omega}_0 t + \phi + \psi) - \sin(\hat{\omega}_0 t + \phi + \psi) - \\
& \left. 3\sin(\hat{\omega}_0 t + \phi - \psi) - \sin(\phi - \psi)\right);
\end{aligned}
$$

- if $\mu = 0$:

$$
\begin{aligned}
u_0(t) &= c_1 t + c_2 \\
u_1(t) &= c_3 t + c_4 \\
&\quad + \frac{\delta}{\hat{\omega}_0^2}\left(-\frac{2c_1}{\hat{\omega}_0}\sin(\hat{\omega}_0 t + \phi) + (c_1 t + c_2)\cos(\hat{\omega}_0 t + \phi)\right).
\end{aligned}
$$

Table A.3: UM method parameters

Symbol	Definition	Eq.
ω	$:= p/(mr_{\text{rest}}^2)$	(19)
$\hat{\omega}_0$	$:= \sqrt{k_{\text{a}}/m + 3\omega^2}$	(19)
ξ	$:= b_{\text{a}}/(2m\hat{\omega}_0)$	(19)
F	$:= -g + r_{\text{rest}}k_{\text{a}}/m + 4r_{\text{rest}}\omega^2$	(19)
ω_{d}	$:= \hat{\omega}_0\sqrt{1-\xi^2}$	(20)
A	$:= r_0 - F/\hat{\omega}_0^2$	(20)
B	$:= (\dot{r}_0 + \xi\hat{\omega}_0 A)/\omega_{\text{d}}$	(20)
M	$:= \sqrt{A^2+B^2}$	(20)
ϕ	$:= \arctan(-B/A)$	(20)
ϕ_2	$:= \arctan(-\sqrt{1-\xi^2}/\xi)$	(21)
z_0	$:= r_{\text{rest}}^2\omega e^{(z_2\cos(\phi-\phi_2))}$	(25)
z_1	$:= \left(3r_{\text{rest}} - 2F/\hat{\omega}_0^2\right) b_{\text{t}}/(mr_{\text{rest}}^3)$	(25)
z_2	$:= -2Mb_t/(mr_{\text{rest}}^3\hat{\omega}_0)$	(25)
z_3	$:= -\omega_{\text{d}}\sin(\phi-\phi_2) - \xi\hat{\omega}_0\cos(\phi-\phi_2)$	(26)
z_4	$:= \cos(\phi-\phi_2)$	(26)
z_5	$:= z_1 + z_2 z_3$	(27)
z_6	$:= z_2 z_4$	(27)
ϕ_3	$:= \arctan\left(\omega_{\text{d}}/(z_5+\xi\hat{\omega}_0)\right)$	(28)
z_7	$:= z_0\left(3r_{\text{rest}} - 2F/\hat{\omega}_0^2\right)/r_{\text{rest}}^3$	(28)
z_8	$:= -2z_0M/\left(r_{\text{rest}}^3\hat{\omega}_0\right)$	(28)
z_9	$:= \theta_0 - z_8\sin\phi$	(28)
z_{10}	$:= z_8\hat{\omega}_0 e^{-z_6}/\sqrt{z_5^2 + 2z_5\xi\hat{\omega}_0 + \hat{\omega}_0^2}$	(28)
z_{11}	$:= \theta_0 - z_{10}\cos(\phi+\phi_3)$	(28)
z_{12}	$:= -z_{10}/\sqrt{z_5^2 + 2z_5\xi\hat{\omega}_0 + \hat{\omega}_0^2}$	(32)
z_{13}	$:= M^2\omega_{\text{d}}^2 b_{\text{a}}/(4\xi\hat{\omega}_0)$	(34)
z_{14}	$:= M^2\xi\hat{\omega}_0 b_{\text{a}}/2$	(34)
z_{15}	$:= M^2\omega_{\text{d}} b_{\text{a}}/4$	(34)
z_{16}	$:= z_{13} + z_{14}\cos^2(\phi+\phi_2) - z_{15}\sin(2\phi+2\phi_2)$	(34)
ϕ_4	$:= \arctan\left(\omega_{\text{d}}/(2z_5+\xi\hat{\omega}_0)\right)$	(35)
z_{17}	$:= 4Mz_0^2 b_{\text{t}} e^{-2z_6}/\left(r_{\text{rest}}^5\sqrt{\omega_{\text{d}}^2 + (2z_5+\xi\hat{\omega}_0)^2}\right)$	(35)
z_{18}	$:= z_0^2(3r_{\text{rest}} - 4F/\hat{\omega}_0^2) b_{\text{t}} e^{-2z_6}/(2r_{\text{rest}}^5 z_5)$	(35)

References

[1] M. H. Raibert, et al., Legged robots that balance, Vol. 3, MIT press Cambridge, MA, 1986.

[2] H. Miura, I. Shimoyama, Dynamic walk of a biped, The International Journal of Robotics Research 3 (2) (1984) 60–74.

[3] R. J. Full, D. E. Koditschek, Templates and anchors: neuromechanical hypotheses of legged locomotion on land, Journal of Experimental Biology 202 (23) (1999) 3325–3332.

[4] R. Alexander, A. Jayes, Vertical movements in walking and running, Journal of Zoology 185 (1) (1978) 27–40.

[5] R. Blickhan, The spring-mass model for running and hopping, Journal of biomechanics 22 (11) (1989) 1217–1227.

[6] R. Altendorfer, U. Saranli, H. Komsuoglu, D. Koditschek, H. B. Brown Jr, M. Buehler, N. Moore, D. McMordie, R. Full, Evidence for spring loaded inverted pendulum running in a hexapod robot, Springer, 2001.

[7] M. Ahmadi, M. Buehler, Controlled passive dynamic running experiments with the ARL-monopod II, IEEE Transactions on Robotics 22 (5) (2006) 974–986.

[8] U. Saranli, M. Buehler, D. E. Koditschek, RHex: A simple and highly mobile hexapod robot, The International Journal of Robotics Research 20 (7) (2001) 616–631.

[9] R. Playter, M. Buehler, M. Raibert, BigDog, in: Pro. of SPIE 6230, Unmanned Systems Technology VIII, 2006, pp. 62302O–62302O.

[10] J. A. Grimes, J. W. Hurst, The design of ATRIAS 1.0 a unique monoped, hopping robot, in: Proceedings of the 2012 International Conference on Climbing and Walking Robots and the Support Technologies for Mobile Machines, 2012, pp. 548–554.

[11] U. Saranli, D. E. Koditschek, Template based control of hexapedal running, in: Proceedings of IEEE International Conference on Robotics and Automation (ICRA), IEEE, 2003, pp. 1374–1379.

[12] H. Geyer, A. Seyfarth, R. Blickhan, Compliant leg behaviour explains basic dynamics of walking and running, Proc. of the Royal Society B: Biological Sciences 273 (1603) (2006) 2861–2867.

[13] S. Collins, A. Ruina, R. Tedrake, M. Wisse, Efficient bipedal robots based on passive-dynamic walkers, Science 307 (5712) (2005) 1082–1085.

[14] J. Rummel, Y. Blum, A. Seyfarth, Robust and efficient walking with spring-like legs, Bioinspiration & biomimetics 5 (4) (2010) 046004.

[15] L. Visser, S. Stramigioli, R. Carloni, Robust bipedal walking with variable leg stiffness, in: Proceedings of 4th IEEE RAS & EMBS International Conference on Biomedical Robotics and Biomechatronics (BioRob), IEEE, 2012, pp. 1626–1631.

[16] G. Garofalo, C. Ott, A. Albu-Schaffer, Walking control of fully actuated robots based on the bipedal SLIP model, in: Proceedings of IEEE International Conference on Robotics and Automation (ICRA), IEEE, 2012, pp. 1456–1463.

[17] J. Ketelaar, L. C. Visser, S. Stramigioli, R. Carloni, Controller design for a bipedal walking robot using variable stiffness actuators, in: Proceedings of IEEE International Conference on Robotics and Automation (ICRA), IEEE, 2013, pp. 5650–5655.

[18] Y. Liu, P. Wensing, D. Orin, Y. Zheng, Dynamic Walking in a Humanoid Robot Based on a 3D Actuated Dual-SLIP Model, in: Proceedings of IEEE International Conference on Robotics and Automation (ICRA), IEEE, 2015, pp. 5710–5717.

[19] M. Shahbazi, R. Babuška, G. A. D. Lopes, Unified Modeling and Control of Walking and Running on the Spring-loaded Inverted Pendulum, IEEE Transactions on Robotics,doi:10.1109/TRO.2016.2593483.

[20] G. Piovan, K. Byl, Approximation and control of the slip model dynamics via partial feedback linearization and two-element leg actuation strategy, IEEE Transactions on Robotics 32 (2) (2016) 399–412.

[21] W. J. Schwind, D. E. Koditschek, Approximating the stance map of a 2-DOF monoped runner, Journal of Nonlinear Science 10 (5) (2000) 533–568.

[22] R. Ghigliazza, R. Altendorfer, P. Holmes, D. Koditschek, A simply stabilized running model, SIAM Journal on Applied Dynamical Systems 2 (2) (2003) 187–218.

[23] H. Geyer, A. Seyfarth, R. Blickhan, Spring-mass running: simple approximate solution and application to gait stability, Journal of theoretical biology 232 (3) (2005) 315–328.

[24] J. J. Robilliard, A. M. Wilson, Prediction of kinetics and kinematics of running animals using an analytical approximation to the planar spring-mass system, Journal of experimental biology 208 (23) (2005) 4377–4389.

[25] H. Yu, M. Li, P. Wang, H. Cai, Approximate Perturbation Stance Map of the SLIP Runner and Application to Locomotion Control, Journal of Bionic Engineering 9 (4) (2012) 411–422.

[26] U. Saranlı, Ö. Arslan, M. M. Ankaralı, Ö. Morgül, Approximate analytic solutions to non-symmetric stance trajectories of the passive spring-loaded inverted pendulum with damping, Nonlinear Dynamics 62 (4) (2010) 729–742.

[27] I. Uyanik, O. Morgul, U. Saranli, Experimental Validation of a Feed-Forward Predictor for the Spring-Loaded Inverted Pendulum Template, IEEE Transactions on Robotics 31 (1) (2015) 208–216.

[28] M. Shahbazi, R. Babuška, G. Lopes, Analytical Approximation for the Double-stance Phase of a Walking Robot, in: Proceedings of IEEE International Conference on Robotics and Automation (ICRA), IEEE, 2015.

[29] Ö. Arslan, U. Saranlı, Reactive planning and control of planar spring–mass running on rough terrain, IEEE Transactions on Robotics 28 (3) (2012) 567–579.

[30] M. Shahbazi, G. Lopes, R. Babuška, Automated Transitions Between Walking and Running in Legged Robots., in: Proceedings of the 19th IFAC World Congress, Vol. 19, 2014, pp. 2171–2176.

[31] O. Arslan, U. Saranli, O. Morgul, An approximate stance map of the spring mass hopper with gravity correction for nonsymmetric locomotions, in: Proceedings of IEEE International Conference on Robotics and Automation (ICRA), IEEE, 2009, pp. 2388–2393.

[32] M. Shahbazi, "Bipedal" Spring-Loaded Inverted Pendulum (SLIP) model and an associated approximate return map in Python (2015). doi:10.4121/uuid:fd95d86d-fa01-4faa-b6e5-eeb92345be8a.

[33] W. J. Schwind, Spring loaded inverted pendulum running: a plant model, Ph.D. thesis, Electrical Enginnering: Systems, University of Michigan (1998).